Electrochimica Acta 58 (2011) 723–728

Contents lists available at SciVerse ScienceDirect

Electrochimica Acta

journal homepage: www.elsevier.com/locate/electacta

Quantifying oxidation rates of carbon monoxide on a Pt/C electrode

S. Balasubramanian, B. Lakshmanan[1], C.E. Hetzke, V.A. Sethuraman[2,3], J.W. Weidner*

Center for Electrochemical Engineering, Department of Chemical Engineering, University of South Carolina, Columbia, SC 29208, USA

ARTICLE INFO

Article history:
Received 19 April 2011
Received in revised form
19 September 2011
Accepted 8 October 2011
Available online 15 October 2011

Keywords:
Carbon monoxide
CO electro-oxidation
Stripping cyclic voltammetry
PEM fuel cells
Platinum poisoning

ABSTRACT

The electrochemical oxidation of carbon monoxide adsorbed (CO_{ad}) on platinum-on-carbon electrodes was studied via a methodology in which pre-adsorbed CO was partially oxidized by applying potentiostatic pulses for certain durations. The residual CO_{ad} was analyzed using stripping voltammetry that involved the deconvolution of CO_{ad} oxidation peaks of voltammograms to quantify the weakly and strongly bound species of CO_{ad}. The data obtained for various potentials and temperatures were fit to a model based on a nucleation and growth mechanism. The resulting fit produced potential- and temperature-dependent rate parameters that provided insight into the oxidation mechanism of the two CO_{ad} species. Irrespective of the applied potential or temperature, the concentration of weakly bound CO_{ad} species decreased exponentially with time. In contrast, the strongly bound CO_{ad} species showed a gradual transition of mechanisms, from progressive nucleation at relatively low potentials to exponential decay at high potentials.

1. Introduction

The presence of carbon monoxide (CO) in hydrogen fed to proton-exchange-membrane fuel cells (PEMFC) (i.e., reformate) has brought considerable attention to understand the kinetics of CO adsorption and oxidation on single and polycrystalline platinum (Pt) electrodes [1]. Various electrochemical and spectral techniques have been employed to: (i) delineate the mechanism of CO poisoning in PEMFC; (ii) estimate the CO induced performance loss in PEMFC; and (iii) develop techniques to mitigate the performance loss [2–7] or remove CO in the fuel stream [8–10]. Developing CO tolerant catalysts or designing electrochemical filters require a quantitative understanding of CO adsorption and electro-oxidation kinetics. In the literature, the kinetic parameters for the electro-oxidation of CO adsorbed on Pt were either measured from electrode-in-solution experiments [11] or deduced from fitting a model to the CO poisoning induced fuel cell performance-loss data [12,13]. However, *in situ* measurements of electro-oxidation kinetic parameters from electrodes reflecting PEMFC are rare due to a complex overlap of different oxidation mechanisms.

The generally accepted mechanism for CO electro-oxidation is the Langmuir–Hinshelwood reaction between adsorbed CO (CO_{ad}) and a neighboring oxygen-containing species, which we refer as OH^*_{ad}, generated from hydrolysis (Eq. (1)) [14].

$$H_2O \rightarrow OH^*_{ad} + H^+ + e^- \quad (1)$$

$$CO_{ad} + OH^*_{ad} \rightarrow CO_2 + H^+ + e^- \quad (2)$$

It has been hypothesized that CO oxidation is limited by the availability of the OH^*_{ad} adjoining a CO_{ad} molecule [15]. Different models proposed to explain the accessibility of the adjacent OH^*_{ad} can be broadly classified into two major groups: nucleation and growth (NG) mechanism and surface diffusion of species. NG mechanism treats the CO_{ad} as stationary species on the Pt surface, and OH^*_{ad} nucleates at specific sites and grows on to consume all of the CO_{ad} [16,17]. The surface diffusion mechanism treats CO_{ad} as mobile species diffusing towards active sites for reaction with OH^*_{ad} [18–28]. Understanding of the mechanism is crucial to understand the activity of electro catalysts. However, it was difficult to arrive at a physically justifiable yet experimentally quantifiable general solution from the models proposed for the electro-oxidation of CO_{ad} on a Pt/C electrode. For example, Friedrich et al. [29] and Koper et al. [18] established the importance of the surface mobility of the species, and their single-crystal electrode studies showed higher activity in kinks rather than terraces supporting the active sites [30]. While Chang et al.'s observation of CO islands supports the NG mechanism [31], NG mechanism could not explain the role of crystalline defects in CO electro-oxidation [28]. As the experimental evidence agrees with each of the models under a limited set of conditions, a single physical model has not been shown to explain

* Corresponding author at: Department of Chemical Engineering, 3C05 Swearingen Engineering Center, University of South Carolina, 315 Main Street, Columbia, SC 29208, USA. Tel.: +1 803 777 3207; fax: +1 803 777 8265.
E-mail address: weidner@cec.sc.edu (J.W. Weidner).
[1] Present address: General Motors Fuel Cell Activities, 10 Carriage Street, Honeoye Falls, NY 14472, USA.
[2] International Society of Electrochemistry Active Member.
[3] Present address: School of Engineering, Brown University, Providence, RI 02912, USA.

0013-4686/$ – see front matter © 2011 Elsevier Ltd. All rights reserved.
doi:10.1016/j.electacta.2011.10.020

the CO electro-oxidation rates under most of the possible conditions.

In addition, CO_{ad} stripping cyclic voltammetry (CO-SCV) on Pt electrodes shows a dual peak response during the electro-oxidation of CO_{ad} [14,32]. Gilman attributed this to the two prominent CO adsorption forms (ad-species) – atop and bridged [14], which were first observed by Eischens and Pliskin through infrared techniques [33], and represented by the superscripts I and II, respectively. Various explanations presented in the literature for the two CO ad-species include: particle size variation [27,34,35], terrace *vs.* edge sites distribution [36], crystallographic orientation [24,28,37], difference in nucleating sites of oxygen-containing species [19] and difference in the mobility of surface species on different crystal facets [38]. The widely accepted view is that the differences in the pattern of adsorption on Pt exhibit the two oxidation peaks in a CO-SCV [5,25,39–50]. By deconvoluting the dual peak in the voltammogram into individual peaks, representing the two ad-species, our group has quantified desorption and rearrangement kinetics of the two CO ad-species over polycrystalline platinum supported on carbon (Pt/C) electrodes [51].

The objective of this work is to develop and test a semi-empirical methodology to understand the potentiostatic oxidation mechanism and quantify the rates for the two distinct CO ad-species on a polycrystalline Pt/C electrode. This was done by quantifying the residual CO_{ad} after applying potentiostatic pulses for certain durations on a Pt/C electrode with pre-adsorbed CO. The residual CO_{ad} is quantified by CO-SCV. The dual peaks observed in the CO-SCV were deconvoluted into two Gaussian peaks representing the two CO ad-species. This procedure was repeated for different pulse durations under a constant potential to obtain the change in the overall CO coverage with pulse time. The electro-oxidation kinetic parameters of the two ad-species were deduced by fitting an equation derived from the NG mechanism with the fractional unreacted CO_{ad} for different pulse durations. The model predictions of the CO ad-species coverage were compared and validated with the individual ad-species coverage estimated from the deconvoluted CO-SCV.

2. Experimental

2.1. Experimental setup

The membrane electrode assembly (MEA) used has a Nafion 115 membrane sandwiched between two polycrystalline Pt/C (XC-72R, E-Tek) electrodes with a Pt loading of 0.5 mg/cm^2 coated over a carbon cloth gas with an area of 10 cm^2. The MEA was assembled into a cell with single-channeled serpentine graphite flow fields. The electrodes were conditioned as reported in our previous work [51]. A gas concentration of 500 ppm of CO in nitrogen, flowing at the rate of 100 cm^3/min for 5 min was used as the CO source to saturate the working electrode. A gas mixture of 4% hydrogen in nitrogen was fed to (100 cm^3/min) the other electrode, which acted as both a counter and reference electrode. All the gases used were procured from Air Products, Inc. and were certified as ultra-high purity. The electrochemical experiments were conducted using a M263A potentiostat/galvanostat from Princeton Applied Research, Inc. and ECHEM software from EG&G.

2.2. CO electro-oxidation and SCV

To estimate the oxidation rate of CO_{ad}, a potentiostatic pulse was applied on a CO-saturated electrode for certain duration, t_d, at a constant temperature, followed by a CO-SCV. The SCV is carried out by scanning the electrode between 50 and 1100 mV with respect to the reference electrode for 3 cycles at a rate of 50 mV/s. The CO-SCV gives the quantity of unreacted CO after the pulse. The change in the quantity of the unreacted CO_{ad} after different pulse durations indicates the oxidation rate of CO_{ad} for that particular applied potential. This procedure of CO saturation and potentiostatic oxidation followed by stripping voltammetry is repeated for pulses of different durations, at different applied potentials in the range of 450–700 mV and for temperatures of 25, 45, 60 and 70 °C.

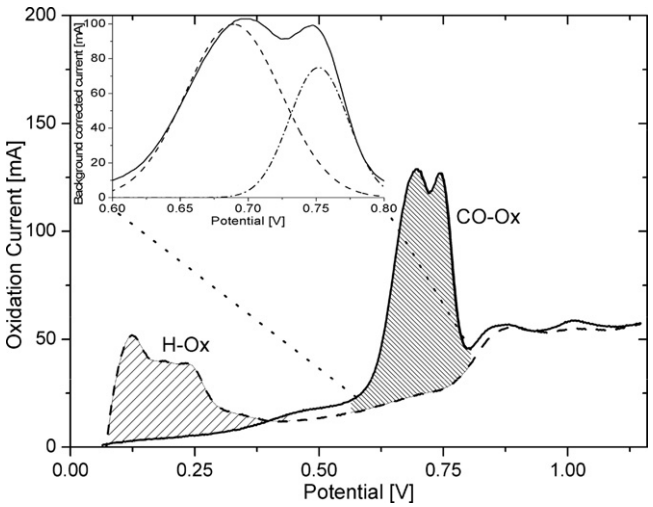

Fig. 1. Anodic scans of cyclic voltammograms obtained on a 40% Pt/C electrode at 45 °C and atmospheric pressure. The dotted line represents Pt and the solid line represents Pt pre-adsorbed with CO. Inset shows the deconvolution of the CO oxidation peaks as two Gaussian peaks.

2.3. Analysis of a CO-SCV

Fig. 1 compares the anodic scans of CO-SCV (line) and a blank with no pre-adsorbed CO (dashed line). Compared to the blank one, hydrogen oxidation (<400 mV) is negligible in the CO-SCV. This is due to the occupation of active sites by CO_{ad}. Whereas in the CO oxidation region (400–900 mV), the dual peaks in CO-SCV represent the electro-oxidation of the two CO ad-species. As the blank did not have CO_{ad}, there was no peak in that potential range. The net charge, corresponding to the area under the dual peak, includes the charge for CO electro-oxidation as in Eqs. (1) and (2). To correct for the background current including double layer capacitance and Pt oxidation, the anodic current response of the blank was subtracted from CO-SCV. The area under the background corrected CO oxidation current is shown as the shaded region in the potential range from 400 to 900 mV. All of the CO oxidation peaks presented henceforth are background corrected CO oxidation peaks obtained from respective CO-SCV.

2.4. Deconvolution of the CO oxidation peaks

The magnified portion of the background corrected CO oxidation peaks is shown in the inset of Fig. 1. The dual peak was deconvoluted as two individual Gaussian peaks representing the two ad-species, CO^{I}_{ad} and. CO^{II}_{ad} For more information on the deconvolution of peaks, please refer to our previous work [51]. The peak at lower potential was assigned to CO^{I}_{ad} and the peak at higher potential was assigned to CO^{II}_{ad}. The oxidation charge for each of the ad-species was estimated by integrating the background corrected and deconvoluted oxidation current peaks over time and was referred as Q^{I} and Q^{II}, respectively. This charge is proportional to the quantity of the unreacted CO ad-species on the Pt/C electrode (Refer Eqs. (1) and (2)). The fractional coverage of unreacted CO_{ad} was estimated by taking the ratio of CO_{ad} coverage after the application of a potential pulse with respect to the saturation CO_{ad} coverage with no pulse applied.

The fractional surface coverage of each of the CO ad-species (θ^{I} and θ^{II}) is defined in Eqs. (3) and (4).

$$\theta^{I} = \frac{Q^{I}}{\left[Q^{I} + Q^{II}\right]_{t=0}} \quad (3)$$

$$\theta^{II} = \frac{Q^{II}}{\left[Q^{I} + Q^{II}\right]_{t=0}} \quad (4)$$

The total initial fractional coverage of CO saturated electrode, when no pulse applied, is taken as unity (i.e., $\theta^{T}_{t=0} = \theta^{I}_{t=0} + \theta^{II}_{t=0} = 1$). The change in the total quantity of CO_{ad} with pulse time is taken as the fractional change in CO_{ad} from the initial saturation CO_{ad} coverage.

2.5. Model equations

The electro-oxidation of CO_{ad} is a surface reaction between CO ad-species and neighboring OH^{*}_{ad} formed from the hydrolysis of water. The oxidation rates of the two CO ad-species are assumed proportional to the rate of change of these individual CO coverages since the rates for desorption and re-arrangement estimated in our previous work [51] are orders of magnitude less than the oxidation rates measured here.

According to NG mechanism, CO_{ad} electro-oxidation rate increases with the rate of nucleation and growth of OH^{*}_{ad} islands and then decreases as these growing OH^{*}_{ad} islands overlap resulting in the shrinkage of CO_{ad} islands [16]. Vollhardt and Retter lumped the nucleation, growth and collapse of islands to a simple expression of fractional coverage as a function of time as [52],

$$\theta_t = \theta_{t=0} \exp(-Kt^{X}) \quad (5)$$

where K is the lumped rate constant and X is the order of time. X indicates the type of NG mechanism and takes the values 1, 2 or 3 for the limiting cases of exponential decay, instantaneous nucleation and progressive nucleation [52], respectively. Here we extend this relationship for two independent populations of CO ad-species to obtain the follow expression for the fractional coverage of CO:

$$\theta^{T}_{t} = \theta^{I}_{t=0} \exp(-K^{I}t^{X^{I}}) + \theta^{II}_{t=0} \exp(-K^{II}t^{X^{II}}) \quad (6)$$

We consider X^{I} and X^{II} as parameters that change with temperature and potential to incorporate the changing nature of oxidation mechanism from progressive nucleation to exponential decay mechanism.

3. Results and discussion

3.1. Effect of oxidation time

Fig. 2 shows the effect of pulse duration on the CO oxidation peaks obtained at 45 °C for the potential 550 mV. With the increase in the duration of potential pulse, the height of the CO oxidation peaks decreased. The height of peak 1 decreased more rapidly than that of peak 2. For the pulse duration of 240 s, the peak 1 is absent indicating a complete oxidation of the. CO^{I}_{ad} The slower oxidation rate of CO^{II}_{ad} indicates the difference in the oxidation rates of the two ad-species.

The integrated total charge under the CO_{ad} oxidation peaks, obtained at 45 °C for different durations of 550 mV potential pulse, were fit to Eq. (6) to obtain and the parameters $K^{I,II}$ and $X^{I,II}$. These data (♦) and the resulting fit (—) are shown in Fig. 3. Also shown in Fig. 3 are the data for the deconvoluted CO_{ad} coverages (Δ, ▲) and those predicted from the individual terms in Eq. (6) (···, —). The excellent agreement between the predictions from the individual terms and the deconvoluted data provide additional confidence in the fit. As seen in Fig. 3, the total coverage rapidly declines during the initial period, followed by a more gradual decline. The sharp initial drop in the overall coverage agrees with the exponential decay in the CO^{I}_{ad} ad-species. The delay in oxidation of the CO^{II}_{ad} ad-species is attributed to slow rate of initiation of the nucleation of the OH^{*}_{ad} islands. This is evident from the fitted values of X for CO^{I}_{ad} and CO^{II}_{ad} ad-species, which are 1 and 2.3 corresponding to exponential decay and nucleation and growth mechanisms, respectively.

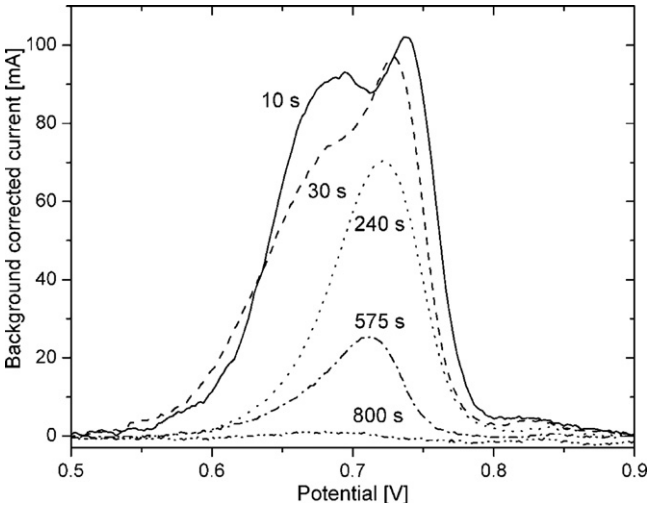

Fig. 2. CO oxidation peaks obtained from baseline corrected CO-SCVs on CO saturated Pt/C electrode after applying pulse potential 550 mV for different durations at 45 °C.

3.2. Effect of applied potential

Fig. 4 shows the base-line corrected CO oxidation peaks obtained after applying pulse potentials (550, 600, 650, 700 mV) for 10 s at 45 °C of the CO saturated Pt electrode. This figure shows the effect of applied potential on the oxidation of CO_{ad} from the electrode surface. With the increase in applied potential, the overall area under the peaks decreased at a faster rate. The first peak decreased rapidly and its contribution was not distinguishable for the CO peaks obtained for the pulse potentials 650 and 700 mV. In addition, as the applied potential was increased, the CO oxidation time

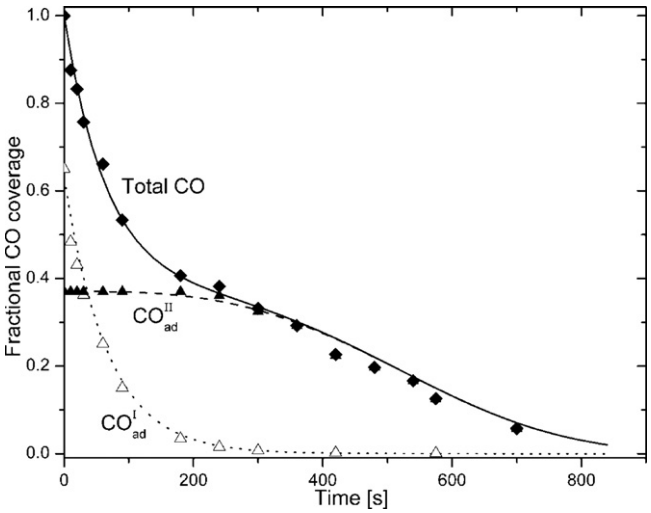

Fig. 3. Comparison of the predicted and experimental fractional CO coverage at 45 °C and for pulse potential of 550 mV. The line represents predictions (---, total CO; ···, CO^{I}_{ad}; —, CO^{II}_{ad}) and symbols show experimental values (♦, total CO; Δ, CO^{I}_{ad}; ▲, CO^{II}_{ad}).

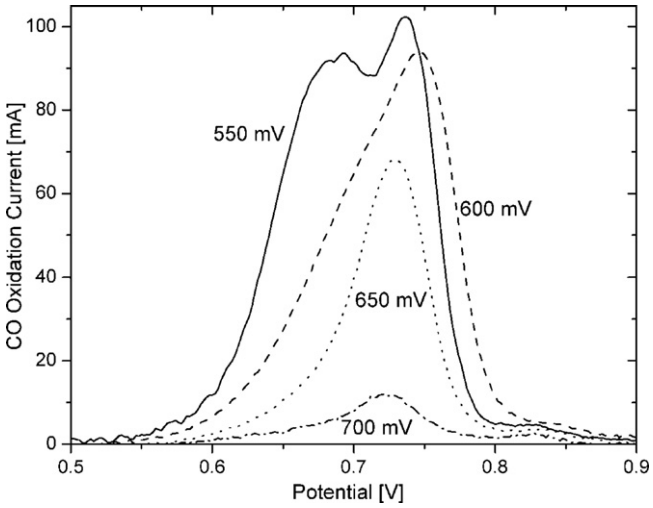

Fig. 4. CO oxidation peaks obtained from baseline corrected CO-SCVs on CO saturated Pt/C electrode after applying pulse potential (550, 600, 650, 700) mV for 10 s at 45 °C.

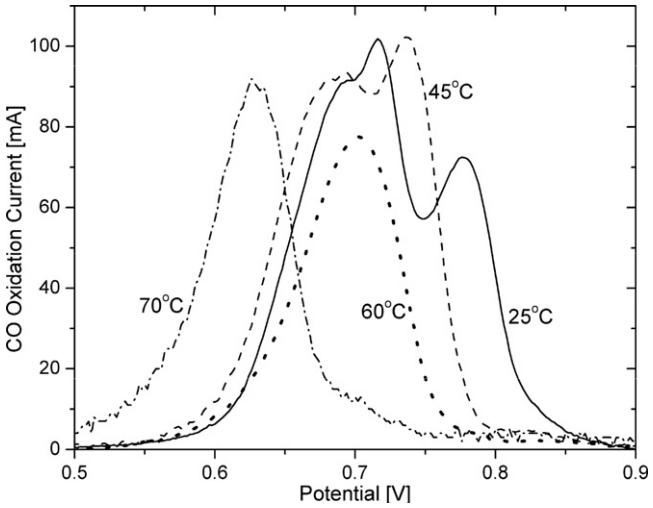

Fig. 6. CO oxidation peaks obtained from baseline corrected CO-SCVs on CO saturated Pt/C electrode after applying pulse potential of 550 mV for 10 s, for temperatures 25, 45, 60 and 70 °C.

decreased. As expected, an increase in the pulse potential promotes the CO oxidation reaction.

Fig. 5 shows the data (symbols) for the fractional coverage *vs.* time for various pulse-potential amplitudes (i.e., 500–700 mV *vs.* DHE) at 45 °C, and Eq. (6) fit to these data (lines). When 500 mV was applied, the CO coverage gradually dropped from around 1.0–0.25 after 800 s. However, when 700 mV was applied within 20 s the coverage dropped to zero. For intermediate cases of 550, 600 and 650 mV pulse, a sharp initial drop followed by a relatively stagnant period and a quick drop in the CO coverage is observed. At lower potentials, both of the CO ad-species oxidize at a very low rate. However as the potential was increased, nucleation of the OH^{*}_{ad} was facilitated near CO^{I}_{ad} ad-species contributing to the increased oxidation of CO^{I}_{ad}, while CO^{II}_{ad} being relatively dormant until the nucleation of OH^{*}_{ad} starts near the CO^{II}_{ad} islands.

3.3. Effect of temperature

The effect of temperature on CO oxidation is shown in Fig. 6. The CO_{ad} oxidation peaks shifted to lower potential with the increase in temperature from 25 °C to 70 °C. Also, the total peak area decreased with increase in the temperature. For example, when the temperature was increased from 25 °C to 60 °C, CO peak area dropped from 688 to 551 mC. The distance between the peak centers decreased with an increase in the temperature. Therefore, two distinguishable peaks at 25 °C converge to indistinguishable peaks at 60 °C.

Eq. (6) was again fit to the fractional CO coverage *vs.* time to obtain $K^{I,II}$ and $X^{I,II}$ as a function of temperature for potentials between 500 and 700 mV. Figs. 7 and 8 show the potential dependence of the fitted parameters K^{I} and K^{II} for different temperatures (25, 45, 60 and 70 °C), respectively. The figures show that the rate constants increase with increasing temperature and oxidation potential for both reactions. The similar slope of the lines for CO^{I}_{ad} oxidation at 25, 45 and 60 °C suggest that the oxidation mechanism is the same over that temperature range. At 70 °C, the slope is noticeable different. For CO^{II}_{ad}, the slopes are fairly constant from 25 to 70 °C.

Fig. 9 shows the temperature and potential dependency of parameters X^{I} (open) and X^{II} (closed) corresponding to the two CO ad-species. The values for X^{I} are approximately 1.0 over the potential and temperature range studied here, suggesting that the

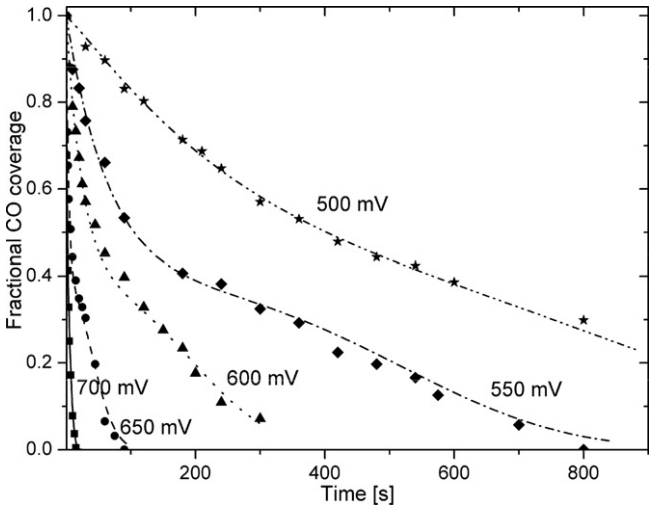

Fig. 5. Comparison of experimental fractional CO coverage (symbols) and fit from Eq. (6) (lines) at 45 °C for pulse potentials of varying amplitudes between 500 and 700 mV *vs.* DHE.

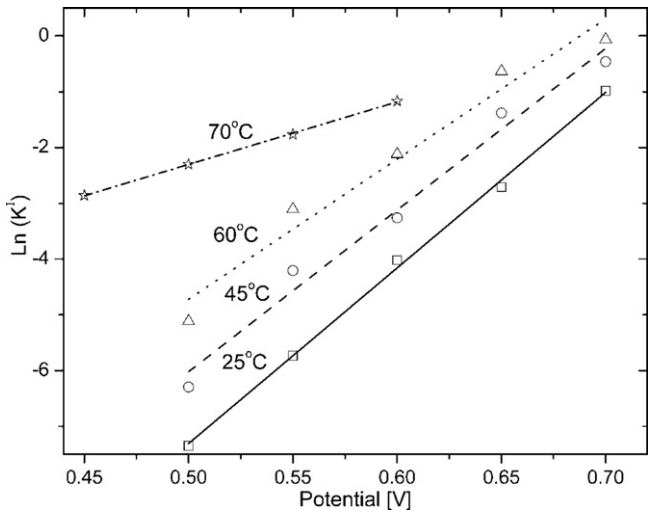

Fig. 7. Dependence of oxidation reaction rate constant (K^{I}) of CO^{I}_{ad} ad-species on the potential for different temperatures (□-25, ○-45, △-60, ☆-70 °C).

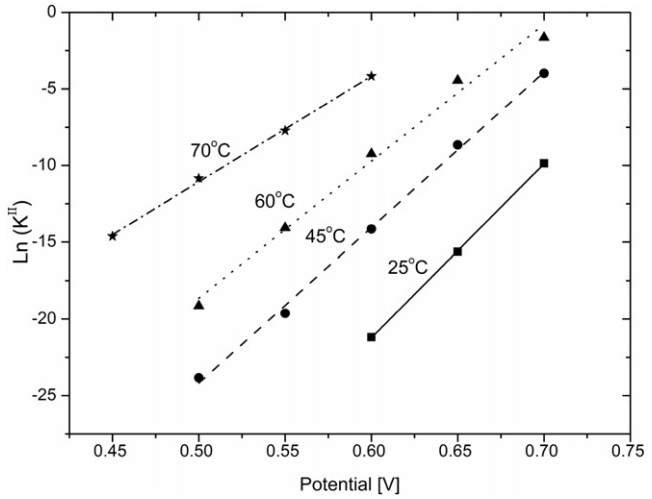

Fig. 8. Dependence of oxidation reaction rate constant (K^{II}) of CO^{II}_{ad} ad-species on the potential for different temperatures (■-25, ●-45, ▲-60, ⋆-70 °C).

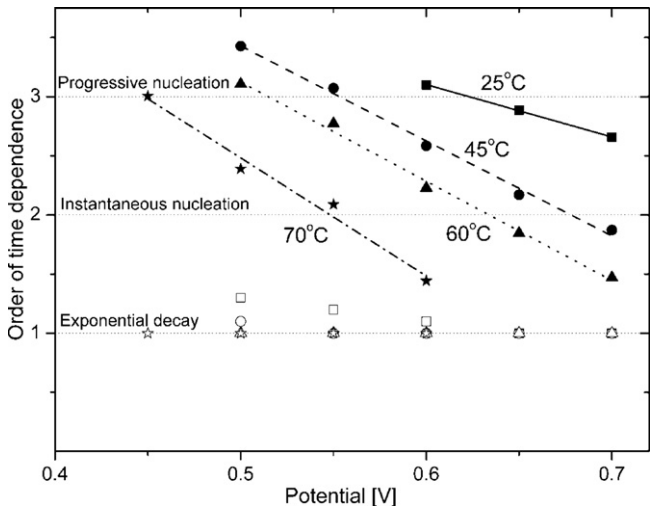

Fig. 9. Order-of-time dependence of X^{I} and X^{II} for CO^{I}_{ad} (open symbols) and CO^{II}_{ad} (closed symbols) ad-species, respectively, on the applied potential for different temperatures in °C (□, ■, 25; ○, ●, 45; △, ▲, 60; ☆, ⋆, 70).

oxidation mechanism for CO^{I}_{ad} is exponential decay. That is, the sites neighboring CO_{ad} contain sufficient OH_{ad} and hence the oxidation rate is limited by the availability of CO_{ad}. Conversely, the value of X^{II} decreased from approximately 3.0 towards 1.0, indicating a shift in the oxidation mechanism from progressive nucleation to exponential decay with increasing potential or temperature. The shift in mechanism is attributed to the increase in availability of sites for OH_{ad} nuclei formation at higher temperatures or potentials. Sufficient OH_{ad} surrounding strongly bound CO^{II}_{ad} leads to a reaction limited by the oxidation of CO^{II}_{ad} with OH_{ad}.

4. Conclusions

A methodology was developed to quantify the electro-oxidation rates of the two CO ad-species on polycrystalline Pt/C porous electrode. CO pre-adsorbed on the electrode was partially oxidized by systematic application of pulse potentials, for certain durations. The residual CO_{ad} was analyzed using stripping voltammetry that involved the deconvolution of CO_{ad} oxidation peaks of voltammograms to quantify the weakly and strongly bound species of CO_{ad}. The changes in the two CO_{ad} coverages *vs.* time were fit to a rate equation based on nucleation and growth mechanism. It was observed that each of the CO ad-species exhibits different oxidation mechanism. We attribute the difference to the formation and accessibility of OH_{ad} to the different ad-species. The oxidation mechanism for the strongly bound ad-species changed from progressive nucleation to exponential decay. The shift in mechanism is attributed to the increasing number of OH_{ad} nuclei with increase in potential. The oxidation mechanism for the weakly bound ad-species exhibited exponential decay over the temperature and potential ranges studied here. Treating the CO oxidation as two distinct ad-species exhibiting different mechanisms helps to overcome the limitation of conventional approaches that explain CO oxidation via a single mechanism. Using the methodology described in this work, CO electro-oxidation can be quantified *in situ* for different electrocatalysts.

Acknowledgement

University of South Carolina assisted in meeting the publication costs of this article.

Appendix A. Nomenclature

List of symbols

Q	Coulombic charge
K	lumped rate constant
X	order of nucleation

Greek symbols

θ	fractional coverage

Super scripts

I	pertaining to first peak
II	pertaining to second peak
T	total CO

Sub scripts

ad	adsorbed
CO	pertaining to CO
t	corresponding to time 't'

References

[1] Y. Morimoto, E.B. Yeager, Journal of Electroanalytical Chemistry 441 (1998) 77.
[2] W.G. Golden, K. Kunimatsu, M.R. Philpott, H. Seki, Abstracts of papers of the American Chemical Society, 188 (1984) 99-Coll.
[3] K. Kunimatsu, W.G. Golden, H. Seki, M.R. Philpott, Langmuir 1 (1985) 245.
[4] M. Avramovivic, R.R. Adzic, A. Bewick, M. Razaq, Journal of Electroanalytical Chemistry 240 (1988) 161.
[5] S.C. Chang, L.-W.H. Leung, M.J. Weaver, The Journal of Physical Chemistry 93 (1989) 5341.
[6] C.K. Rhee, J.M. Feliu, E. Herrero, P. Mrozek, A. Wieckowski, Journal of Physical Chemistry 97 (1993) 9730.
[7] E. Zippel, R. Kellner, M. Krebs, M.W. Breiter, Journal of Electroanalytical Chemistry 330 (1992) 521.
[8] L.A. Balasubramanian, W. Huang, J.W. Weidner, Electrochemical Solid State Letters 5 (2002) A267–A270.
[9] S. Balasubramanian, C.E. Holland, J.W. Weidner, Electrochemical and Solid-State Letters 13 (2010) B5–B7.
[10] L.P.L. Carrette, K.A. Friedrich, M. Huber, U. Stimming, Physical Chemistry Chemical Physics 3 (2001) 320.
[11] S.A. Bilmes, A.J. Arvia, Journal of Electroanalytical Chemistry 361 (1993) 159.
[12] T.E. Springer, T. Rockward, T.A. Zawodzinski, S. Gottesfeld, Journal of the Electrochemical Society 148 (2001) A11–A23.
[13] J.J. Baschuk, X.G. Li, International Journal of Energy Research 25 (2001) 695.
[14] S. Gilman, The Journal of Physical Chemistry 67 (1963) 78.
[15] O.V. Cherstiouk, P.A. Simonov, V.I. Zaikovskii, E.R. Savinova, Journal of Electroanalytical Chemistry 554 (2003) 241.
[16] C. Mccallum, D. Pletcher, Journal of Electroanalytical Chemistry 70 (1976) 277.
[17] B. Love, J. Lipkowski, ACS Symposium Series 378 (1988) 484.

[18] M.T.M. Koper, N.P. Lebedeva, C.G.M. Hermse, Faraday Discussions 121 (2002) 301.
[19] F. Maillard, M. Eikerling, O.V. Cherstiouk, S. Schreier, E. Savinova, U. Stimming, Faraday Discussions 125 (2004) 357.
[20] M. Metikos-Hukovic, S. Omanovic, Journal of Molecular Catalysis A: Chemical 136 (1998) 75.
[21] S.K. Desai, M. Neurock, Physical Review B 68 (2003).
[22] M. Bergelin, E. Herrero, J.M. Feliu, M. Wasberg, Journal of Electroanalytical Chemistry 467 (1999) 74.
[23] N.P. Lebedeva, M.T.M. Koper, J.M. Feliu, R.A. van Santen, Journal of Electroanalytical Chemistry 524 (2002) 242.
[24] J. Solla-Gullon, F.J. Vidal-Iglesias, E. Herrero, J.M. Feliu, A. Aldaz, Electrochemistry Communications 8 (2006) 189.
[25] N.M. Markovic, B.N. Grgur, C.A. Lucas, P.N. Ross, Journal of Physical Chemistry B 103 (1999) 487.
[26] F. Maillard, S. Schreier, M. Hanzlik, E.R. Savinova, S. Weinkauf, U. Stimming, Physical Chemistry Chemical Physics 7 (2005) 385.
[27] F. Maillard, E.R. Savinova, P.A. Simonov, V.I. Zaikovskii, U. Stimming, Journal of Physical Chemistry B 108 (2004) 17893.
[28] N.P. Lebedeva, M.T.M. Koper, J.M. Feliu, R.A. van Santen, Journal of Physical Chemistry B 106 (2002) 12938.
[29] K.A. Friedrich, K.P. Geyzers, U. Linke, U. Stimming, J. Stumper, Journal of Electroanalytical Chemistry 402 (1996) 123.
[30] G. Garcia, M.T.M. Koper, Physical Chemistry Chemical Physics 10 (2008) 3802.
[31] S.C. Chang, M.J. Weaver, Journal of Chemical Physics 92 (1990) 4582.
[32] S. Gilman, The Journal of Physical Chemistry 66 (1962) 2657.
[33] R.D. Eischens, W. Pliskin, Advances in Catalysis, Academic Press, Inc., New York, NY, 1958.
[34] O.V. Cherstiouk, P.A. Simonov, E.R. Savinova, Electrochimica Acta 48 (2003) 3851.
[35] K.A. Friedrich, F. Henglein, U. Stimming, W. Unkauf, Colloids and Surfaces A: Physicochemical and Engineering Aspects 134 (1998) 193.
[36] S. Guerin, B.E. Hayden, C.E. Lee, C. Mormiche, J.R. Owen, A.E. Russell, B. Theobald, D. Thompsett, Journal of Combinatorial Chemistry 6 (2004) 149.
[37] K.J.J. Mayrhofer, M. Arenz, B.B. Blizanac, V. Stamenkovic, P.N. Ross, N.M. Markovic, Electrochimica Acta 50 (2005) 5144.
[38] V.P. Zhdanov, B. Kasemo, Chemical Physics Letters 376 (2003) 220.
[39] F. Kitamura, M. Takahashi, M. Ito, Surface Science 223 (1989) 493.
[40] D. Kardash, J.M. Huang, C. Korzeniewski, Langmuir 16 (2000) 2019.
[41] B. Beden, F. Hahn, J.M. Leger, C. Lamy, C.L. Perdriel, N.R. Detacconi, R.O. Lezna, A.J. Arvia, Journal of Electroanalytical Chemistry 301 (1991) 129.
[42] D. Kardash, C. Korzeniewski, Langmuir 16 (2000) 8419.
[43] I. Villegas, M.J. Weaver, The Journal of Chemical Physics 101 (1994) 1648.
[44] K. Kunimatsu, H. Seki, W.G. Golden, J.G. Gordon, M.R. Philpott, Langmuir 2 (1986) 464.
[45] J. Sobkowski, A. Czerwinski, The Journal of Physical Chemistry 89 (1985) 365.
[46] B. Beden, C. Lamy, N.R. de Tacconi, A.J. Arvia, Electrochimica Acta 35 (1990) 691.
[47] V.E. Kazarinov, V.N. Andreev, A.V. Shlepakov, Electrochimica Acta 34 (1989) 905.
[48] A. Couto, M.C. Perez, A. Rincon, C. Gutierrez, Journal of Physical Chemistry 100 (1996) 19538.
[49] A. Wieckowski, M. Rubel, C. Gutierrez, Journal of Electroanalytical Chemistry 382 (1995) 97.
[50] H. Kita, H. Naohara, T. Nakato, S. Taguchi, A. Aramata, Journal of Electroanalytical Chemistry 386 (1995) 197.
[51] V.A. Sethuraman, B. Lakshmanan, J.W. Weidner, Electrochimica Acta 54 (2009) 5492.
[52] D. Vollhardt, U. Retter, The Journal of Physical Chemistry 95 (1991) 3723.